

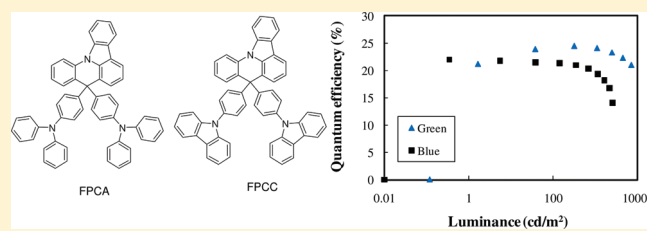
Indolo Acridine-Based Hole-Transport Materials for Phosphorescent OLEDs with Over 20% External Quantum Efficiency in Deep Blue and Green

Min Su Park and Jun Yeob Lee*

Department of Polymer Science and Engineering, Dankook University 126, Jukjeon-dong, Suji-gu, Yongin, Gyeonggi, 448-701, Korea

ABSTRACT: Thermally stable high-triplet-energy hole transport materials based on 8H-indolo[3,2,1-de]acridine core (FPC) were synthesized and the device performances of FPC-based phosphorescent organic light-emitting diodes (OLEDs) were investigated. The FPC-based hole transport materials showed a high triplet energy (above 2.90 eV) and high glass-transition temperature (above 140 °C). The FPC-based hole-transport materials (HTMs) were effective as the HTMs for green and deep-blue phosphorescent OLEDs, and a high quantum efficiency (over 20%) was achieved in both devices.

KEYWORDS: high quantum efficiency, high triplet energy, hole transport material, thermal stability



INTRODUCTION

Phosphorescent organic light-emitting diodes (PHOLEDs) have been developed for more than 10 years, because of their merit of high quantum efficiency.¹ Over 20% external quantum efficiency has already been reported in red/green/blue PHOLEDs, although the high efficiency was hardly reported in deep-blue PHOLEDs.^{2–5}

There are several factors affecting the quantum efficiency of PHOLEDs, which include charge balance in the emitting layer, triplet exciton blocking, and triplet energy transfer. In particular, the triplet exciton blocking was critical to the quantum efficiency of PHOLEDs.^{6–12} The lifetime of triplet excitons (on the scale of microseconds) is much longer than that of the singlet excitons (on the scale of nanoseconds). Therefore, the triplet excitons can diffuse out of the emitting layer and be quenched by the charge transport layer.¹⁰ The triplet exciton quenching can be suppressed by using a high-triplet-energy exciton blocking layer, which has higher triplet energy than the emitting material.

Both hole-transport-type and electron-transport-type exciton blocking materials have been developed to improve the quantum efficiency of PHOLEDs. Various carbazole- or aromatic amine-based hole transport materials (HTMs) have been successful to block triplet excitons,^{9,13} and imidazole-, triazole-, or oxadiazole-type electron transport materials could suppress the triplet exciton diffusion.^{4–7,11} The quantum efficiency could be greatly enhanced by using the high-triplet-energy exciton blocking layers.

However, it was difficult to develop an exciton blocking layer for deep-blue PHOLEDs. Deep-blue-emitting phosphorescent dopants have a triplet energy over 2.7 eV and the exciton blocking material should have a triplet energy over 2.8 eV for efficient triplet exciton blocking. *N,N'*-dicarbazolyl-3,5-benzene (*mCP*),^{14,15} 1,1-bis[(di-4-tolylamino)phenyl]cyclohexane (TAPC),⁵ 2,2'-bis(4-ditolylaminophenyl)-1,1'-biphenyl,¹⁶ 2,2'-bis(3-ditolylaminophenyl)-1,1'-biphenyl,¹⁶ and bis[4-(*p,p'*-ditolylamino)-phenyl]diphenylsilane¹⁷

have been used as high-triplet-energy HTMs for blue PHOLEDs, because of the high triplet energy of 2.9 eV. However, *mCP* has a problem of poor thermal stability and TAPC has a problem of improper highest occupied molecular orbital (HOMO) level for hole injection. The HOMO level of TAPC is approximately -5.5 eV and hole injection from TAPC to deep-blue host materials with a HOMO level below -6.0 eV is difficult, because of the high energy barrier for hole injection. Other compounds could not be applied in deep-blue PHOLEDs, because of low triplet energy or poor hole injection. Therefore, it is strongly required to develop thermally stable high-triplet-energy HTMs for efficient charge injection and triplet exciton blocking in deep-blue PHOLEDs.

In this work, thermally stable high-triplet-energy HTMs based on an 8H-indolo[3,2,1-de]acridine (FPC) core will be synthesized, and the device performances of the deep blue and green PHOLEDs are investigated. Over 20% external quantum efficiency in deep-blue and green PHOLEDs were demonstrated using the FPC-based HTMs.

EXPERIMENTAL SECTION

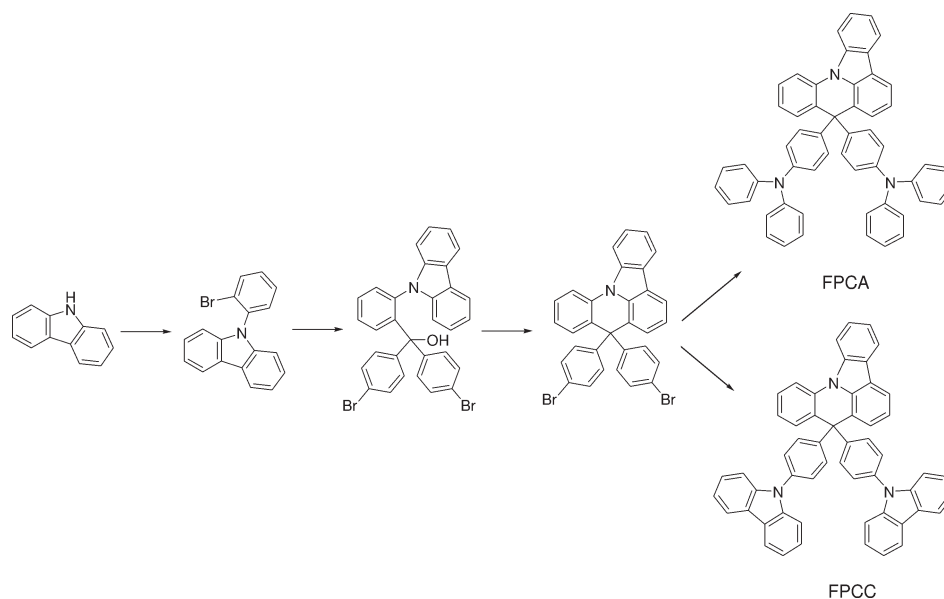
General Information. The following chemicals (from Aldrich Chemical Co.) were used without further purification: 9H-carbazole, *n*-butyllithium, dichlorobenzene, copper iodide(I), and 18-crown-6. Hydrogen chloride (Duksan Science Co.), potassium carbonate (Duksan Science Co.), 1-bromo-2-iodobenzene (TCI Chemical Co.), and 4,4'-dibromobenzophenone (Alfa Aesar. Co.) also were used as received. Tetrahydrofuran (THF) was distilled over sodium and calcium hydride.

Received: June 9, 2011

Revised: August 22, 2011

Published: September 06, 2011

Scheme 1. Synthetic Scheme of FPCA and FPCC



Nuclear magnetic resonance (^1H NMR and ^{13}C NMR) spectra were recorded on a Varian 200 (200 MHz) spectrometer. A fluorescence spectrophotometer (Hitachi, Model F-7000) and ultraviolet–visible light (UV–vis) spectrophotometer (Shimadzu, Model UV-2501PC) were used to measure the photoluminescence (PL) spectra and UV–vis spectra. Low-temperature PL measurement of the synthesized materials was carried out at 77 K, using a dilute solution of the materials. The differential scanning calorimeter (DSC) measurements were performed using a Mettler Model DSC 822e system under nitrogen at a heating rate of $10\text{ }^\circ\text{C}/\text{min}$. The mass spectra were recorded using a JEOL Model JMS-AXS05WA spectrometer in fast-atom bombardment (FAB) mode. The HOMO energy levels were measured using cyclic voltammetry (CV). CV measurement of the organic materials was carried out in acetonitrile solution with tetrabutylammonium perchlorate at 0.1 M concentration. Silver was used as the reference electrode, and platinum was used as the counter electrode. Organic materials were coated on an indium tin oxide (ITO) substrate and were immersed in electrolyte for analysis.

Synthesis. Synthetic scheme of the FPC compounds is described in Scheme 1. The synthesis of the intermediate compound was reported in other work.¹⁸

Synthesis of 8,8-bis(4-(9H-carbazol-9-yl)phenyl)-8H-indolo[3,2,1-de]acridine (FPCC). 9H-Carbazole (0.736 g, 4.422 mmol), 8,8-bis(4-bromophenyl)-8H-indolo[3,2,1-de]acridine (1 g, 1.76 mmol), potassium carbonate (0.51 g, 3.70 mmol), copper(I) iodide (0.085 g, 0.442 mmol), and dibenzo 18-crown-6 (0.046 g, 0.176 mmol) were dissolved in dimethylformamide (DMF) under a nitrogen atmosphere. The reaction mixture was stirred for 12 h at $100\text{ }^\circ\text{C}$. The mixture was diluted with dichloromethane and washed with distilled water (100 mL) three times. The organic layer was dried over anhydrous MgSO_4 and evaporated in vacuo to give the crude product. The extract was evaporated to dryness, affording a white solid (0.849 g), which was further purified by column chromatography, using dichloromethane/*n*-hexane.

Yield, 65%; T_g , $149\text{ }^\circ\text{C}$. ^1H NMR (200 MHz, CDCl_3): δ 8.25 (d, 1H, $J = 8.0\text{ Hz}$), 8.21 (d, 1H, $J = 8.0\text{ Hz}$), 8.13 (d, 2H, $J = 8.0\text{ Hz}$), 8.05 (d, 1H, $J = 8.0\text{ Hz}$), 7.64–7.20 (m, 30H). ^{13}C NMR (50 MHz, CDCl_3): δ 145.4, 141.1, 139.1, 138.0, 137.5, 136.6, 132.9, 132.4, 131.9, 131.5, 128.9, 127.8, 127.2, 126.8, 126.0, 125.7, 123.8, 122.7, 122.3, 121.3, 120.9, 120.1, 119.8, 119.5, 118.5, 115.4, 114.8, 114.2, 113.8, 110.8, 109.7, 57.1. MS (FAB) m/z 737 [(M + H) $^+$]. Anal. Calcd for $\text{C}_{55}\text{H}_{35}\text{N}_3$: C, 89.52; H, 4.78; N, 5.69. Found: C, 89.17; H, 4.73; N, 5.71.

4,4'-(8H-indolo[3,2,1-de]acridine-8,8-diyl)bis(N,N-diphenylaniline) (FPCA). Diphenylamine (0.748 g, 4.422 mmol), 8,8-bis(4-bromophenyl)-8H-indolo[3,2,1-de]acridine (1 g, 1.76 mmol), potassium carbonate (0.51 g, 3.70 mmol), copper(I) iodide (0.085 g, 0.442 mmol), and dibenzo 18-crown-6 (0.046 g, 0.176 mmol) were dissolved in *o*-dichlorobenzene under nitrogen atmosphere. The reaction mixture was stirred for 12 h at $100\text{ }^\circ\text{C}$. The mixture was diluted with dichloromethane and washed with distilled water (100 mL) three times. The organic layer was dried over anhydrous MgSO_4 and evaporated in vacuo to give the crude product. The extract was evaporated to dryness, affording a white solid (0.852 g), which was further purified by column chromatography, using dichloromethane/*n*-hexane.

Yield, 65%; T_g , $142\text{ }^\circ\text{C}$. ^1H NMR (200 MHz, CDCl_3): δ 8.13 (d, 1H, $J = 8.0\text{ Hz}$), 8.09 (d, 1H, $J = 8.0\text{ Hz}$), 7.95 (d, 1H, $J = 8.0\text{ Hz}$), 7.74–7.62 (m, 3H), 7.56–7.46 (m, 5H), 7.40–6.80 (m, 28H). ^{13}C NMR (50 MHz, CDCl_3): δ 148.1, 146.4, 140.4, 139.0, 138.0, 137.3, 132.7, 131.7, 130.7, 130.1, 129.0, 128.4, 127.2, 126.1, 125.3, 124.4, 123.7, 123.1, 122.7, 122.2, 121.0, 119.0, 117.9, 115.5, 114.5, 113.5, 56.2. MS (FAB) m/z 741 [(M + H) $^+$]. Anal. Calcd for $\text{C}_{55}\text{H}_{39}\text{N}_3$: C, 89.02; H, 5.30; N, 5.66. Found: C, 89.12; H, 5.51; N, 5.41.

Device Fabrication and Measurements. The device structure of blue PHOLEDs was indium tin oxide (ITO, 150 nm)/*N,N'*-diphenyl-*N,N'*-bis-[4-(phenyl-*m*-tolyl-amino)-phenyl]-biphenyl-4,4'-diamine (DNTPD, 60 nm)/*N,N'*-di(1-naphthyl)-*N,N'*-diphenylbenzidine (NPB, 5 nm)/FPCC or FPCA (10 nm)/9-(3-(9H-carbazol-9-yl)phenyl)-3-(dibromophenylphosphoryl)-9H-carbazole (*m*CPPO1):bis((3,5-difluoro-4-cyanophenyl)pyridine) iridium picolinate (FCNirpic) (30 nm, 3%)/diphenylphosphine oxide-4-(triphenylsilyl)phenyl (TSPO1, 25 nm)/LiF(1 nm)/Al(200 nm). Green PHOLED had the device structure of ITO (150 nm)/DNTPD (60 nm)/NPB (20 nm)/FPCA or FPCC (10 nm)/bis-9,9'-spiro[fluoren-2-yl]-methanone (BSFM):tris(2-phenylpyridine) iridium ($\text{Ir}(\text{ppy})_3$)/TSPO1 (25 nm)/LiF (1 nm)/Al (200 nm). The device performances of the blue and green PHOLEDs were measured with Keithley Instruments Model 2400 source measurement unit and Model CS1000 spectroradiometer.

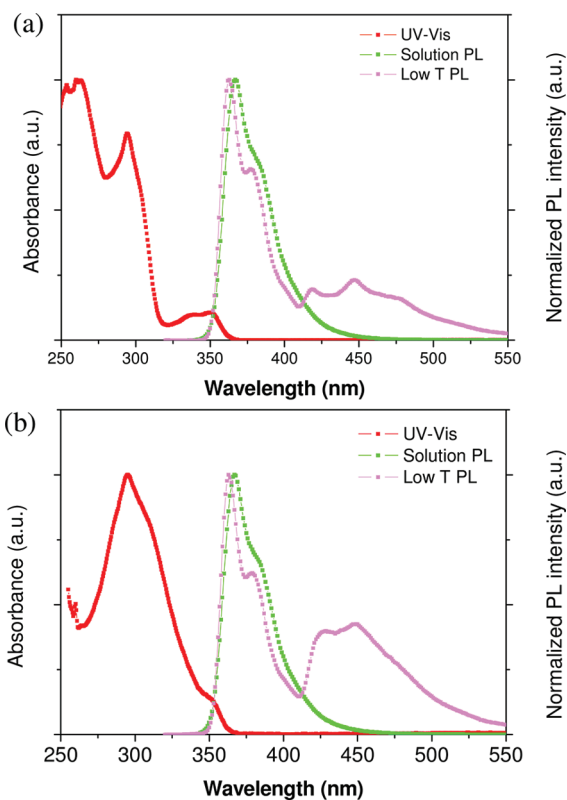
RESULTS AND DISCUSSION

Two FPC-based HTMs were synthesized; the synthetic scheme of the materials has already been shown in Scheme 1.

Table 1. Photophysical properties of FPCA and FPCC

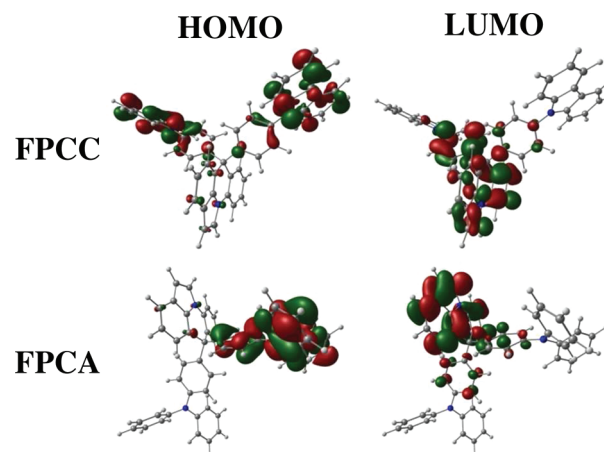
	UV-vis (nm) ^a	PL (nm) ^b	T _g (°C)	HOMO (eV)	LUMO (eV)	bandgap (eV)	E _T (eV)
FPCA	259	368	142	-5.78	-2.42	3.36	2.90
FPCC	295	366	149	-6.03	-2.65	3.38	2.96

^a Ultraviolet-visible light spectroscopy. Tetrahydrofuran (THF) was used as the solvent. ^b Photoluminescence. Tetrahydrofuran (THF) was used as the solvent.

**Figure 1.** UV-vis absorption and PL spectra of (a) FPCC and (b) FPCA.

The FPC was designed as the high-triplet-energy core with high-temperature stability. The FPC core can have the high triplet energy of phenylcarbazole, because the conjugation of the phenylcarbazole is not extended through the sp³ carbon. In addition, it can show high-temperature stability as the rotation of the phenyl group is limited by the additional bond between the phenyl and carbazole groups. Based on the rigid FPC core, two different hole transport units—FPCA and FPCC—were introduced in the molecular structure, to improve the hole transport properties.

Physical properties of the HTMs were analyzed and are summarized in Table 1. Two materials showed different UV-vis absorption and PL spectra (Figure 1). The UV-vis absorption of the FPCC is from $\pi-\pi^*$ transition of the carbazole and 8H-indolo[3,2,1-de]acridine moieties, while that of FPCA is from $\pi-\pi^*$ transition of the 8H-indolo[3,2,1-de]acridine and the diphenylamine unit. In addition to the main absorption peak at 295 nm, which is attributed to the 8H-indolo[3,2,1-de]acridine group, the FPCA showed a shoulder peak that originated from the aromatic amine group at long wavelength. The PL spectra were slightly red-shifted in the FPCA, because of the aromatic amine unit. The HOMO and the lowest unoccupied molecular

**Figure 2.** Molecular orbital simulation results of FPCA and FPCC.

orbital (LUMO) of the FPC-based HTMs were measured from the absorption edge of the UV-vis absorption and oxidation potential from CV. The HOMO level of the FPCA was -5.78 eV, while that of the FPCC was -6.03 eV. The HOMO level of the FPCA was shifted upward by 0.25 eV, compared to that of the FPCC. As can be seen in the molecular orbital distribution of the FPCA and FPCC (Figure 2), the HOMO is localized on the aromatic amine and carbazole units of each molecule. Therefore, the HOMO level was upward shifted in the FPCA, because of the strong electron-donating character of the aromatic amine unit. The bandgaps were calculated from the UV-vis absorption edge of the HTMs; they were determined to be 3.36 and 3.39 eV. Considering the bandgap of the FPCA and FPCC, the LUMO levels were -2.42 eV and -2.65 eV for FPCA and FPCC, respectively. The triplet energies of the HTMs were measured from low-temperature PL spectra and they were 2.90 and 2.96 eV for FPCA and FPCC, respectively. The triplet energy of the two HTMs was high enough for triplet exciton blocking in deep-blue PHOLEDs. Therefore, two HTMs were adopted as the hole-transport-type exciton blocking layer in deep-blue and green PHOLEDs. The glass-transition temperatures (T_g) of the FPCC and FPCA are also presented in Table 1. Both compounds showed high T_g values (over 140 °C), because a rigid core structure was introduced in the FPCC and FPCA. Therefore, the use temperature of the FPCA and FPCC HTMs can be as high as 140 °C. In particular, the FPCC showed a high T_g value of 149 °C, because of the rigid aromatic carbazole unit. The thermal stability of the two materials were tested at 100 °C for 10 min and two materials did not show any change of the film morphology even after thermal treatment, demonstrating the thermal stability of the FPCC and FPCA.

Deep-blue PHOLEDs with a device configuration of ITO/DNTPD/NPB/FPCC or FPCA/mCPPO1:FCNIRpic/TSP01/LiF/Al were fabricated and device performances were investigated.

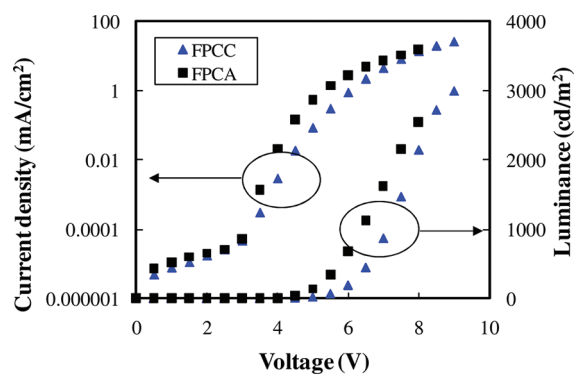


Figure 3. Current density–voltage–luminance data of blue PHOLEDs with FPCC and FPCA.

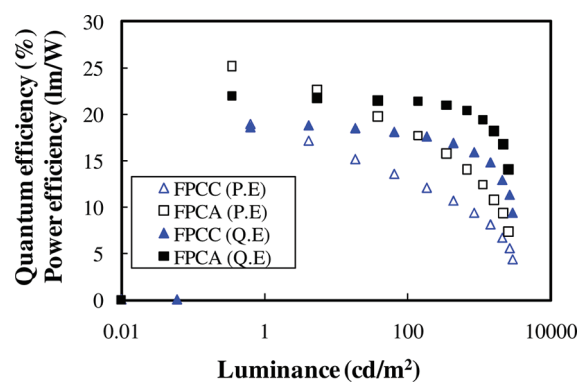


Figure 6. Quantum efficiency–luminance and power efficiency–luminance curves of blue PHOLEDs with FPCC and FPCA.

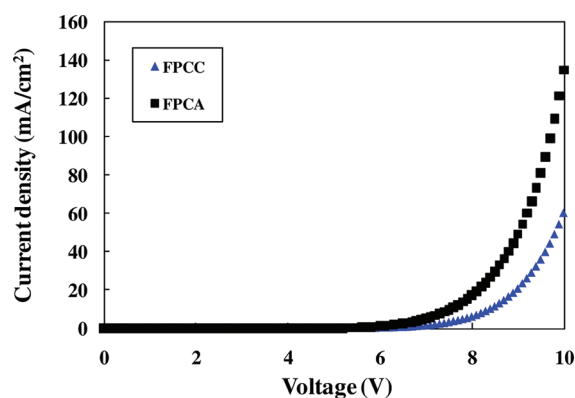


Figure 4. Current density–voltage curves of hole-only devices of FPCC and FPCA.

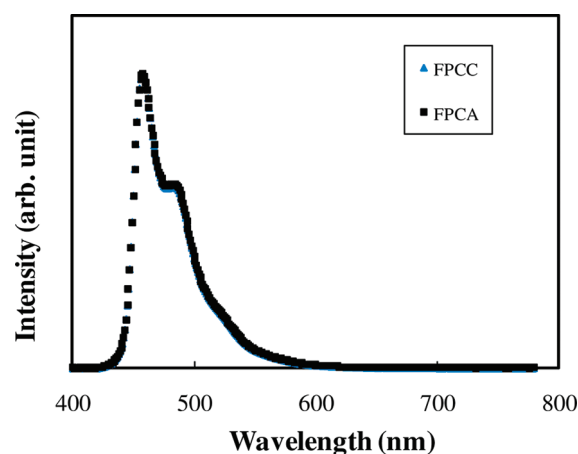


Figure 7. Electroluminescence spectra of blue PHOLEDs with FPCC and FPCA.

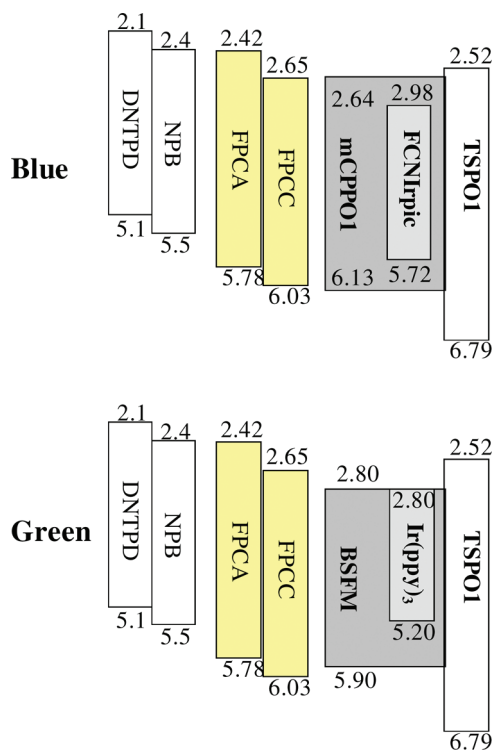


Figure 5. Energy-level diagram of blue and green phosphorescent organic light-emitting diodes (PHOLEDs).

The FPCA and FPCC have the HOMO levels of -5.78 eV and -6.03 eV for hole injection from NPB (-5.5 eV) to *m*CPPO1 (-6.13 eV) and high triplet energy over 2.90 eV for triplet exciton blocking. Therefore, high quantum efficiency can be obtained from the deep-blue PHOLED, using the FPC-based HTMs. Figure 3 shows the current density–voltage–luminance curves of the deep-blue PHOLEDs. The FPCA device showed higher current density than FPCC device. The difference of the current density is due to the different hole density in the emitting layer as the same electron transport layer was used in two devices. Therefore, this result indicates that the FPCA is better than FPCC in terms of hole transport.

To confirm the hole-transport properties, hole-only devices of two HTMs were fabricated and the hole current density was compared. Figure 4 shows the current density–voltage curves of the hole-only device of two HTMs. The device structure was ITO/DNTPD (60 nm)/NPB (5 nm)/FPCA or FPCA (30 nm)/Au. The hole current density was increased in the order of FPCA > FPCC. As expected, the hole current density showed the same tendency as the current density of PHOLEDs. In general, the hole current density depends on the energy level and hole-transport properties of the materials. Considering the HOMO level, FPCA is better than FPCC, because the energy barriers for hole injection from NPB to HTMs were 0.28 and 0.53 eV for FPCA and FPCC, respectively. FPCA is better than

Table 2. Device Performances of FPCA and FPCC Blue and Green Devices

	driving voltage (V) ^a	maximum quantum efficiency (%)	quantum efficiency (%) ^a	maximum power efficiency (lm/W)	power efficiency (lm/W) ^a	maximum current efficiency (cd/A)	color coordinate ^a
Blue-FPCA	6.3	22.0	19.7	25.2	13.0	26.0	(0.14, 0.17)
Blue-FPCC	7.1	18.8	15.6	19.0	9.1	22.3	(0.14, 0.17)
Green-FPCA	5.4	24.5	24.2	58.5	50.1	79.0	(0.33, 0.62)
Green-FPCC	6.2	24.3	21.1	54.4	37.0	78.3	(0.33, 0.62)

^a Measured at 1000 cd/m².

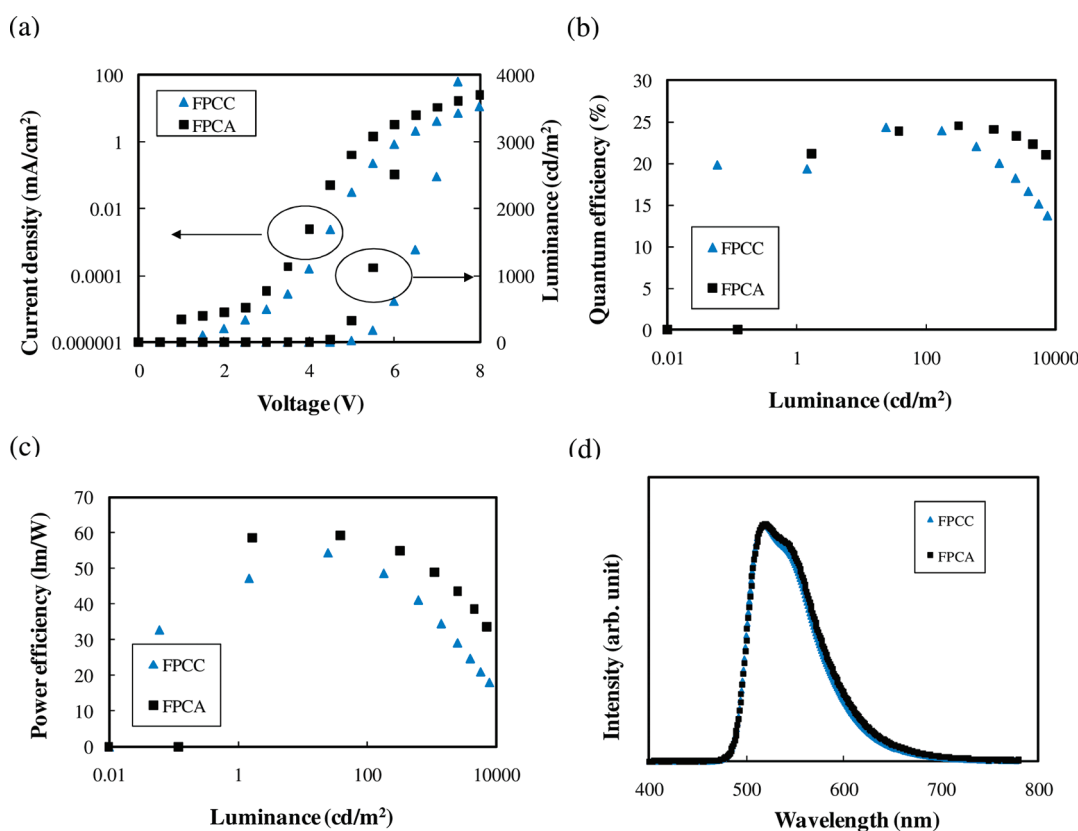


Figure 8. (a) Current density–voltage–luminance, (b) quantum efficiency–luminance, (c) power efficiency–luminance, and (d) electroluminescence data of green PHOLEDs with FPCA and FPCC HTMs.

FPCC, in terms of hole transport, because it is well-known that the order of hole-transport character is amine > carbazole. The hole mobility of FPCA ($1.4 \times 10^{-3} \text{ cm}^2/(\text{V s})$) was higher than that of the FPCC ($5.2 \times 10^{-4} \text{ cm}^2/(\text{V s})$). The order of hole-transport character coincided with the hole current density of the hole-only devices. Therefore, the different current density of the deep-blue PHOLEDs is due to different hole-transport character of the high-triplet-energy HTMs and energy barrier for hole injection. The energy level diagram of the devices is shown in Figure 5.

The quantum efficiency–luminance and power efficiency–luminance data are shown in Figure 6. The quantum efficiency of the deep-blue PHOLEDs was on the order of FPCA > FPCC. The *m*CPPO1 host has rather strong electron transport properties, because of the diphenylphosphine oxide group. Therefore, more hole injection can improve the quantum efficiency of the deep-blue PHOLEDs. Because the FPCA showed better hole-injection properties than FPCC, the quantum efficiency of the FPCA device was higher than that of FPCC. The maximum

external quantum efficiency of the FPCA device was 22.0%, and the quantum efficiency at 1000 cd/m² was 19.7%. The maximum power efficiency was 25.2 lm/W, and the power efficiency at 1000 cd/m² was 13.0 lm/W. The color coordinate of the device was (0.14, 0.17), as shown in the electroluminescence spectra (see Figure 7). Detailed device data are summarized in Table 2.

The high quantum and power efficiencies of the deep-blue PHOLEDs with the FPCA can be explained by the high recombination efficiency and triplet exciton blocking. The recombination efficiency was improved because of efficient hole injection from FPCA to the *m*CPPO1 emitting layer. In addition, the triplet exciton quenching by the HTMs was suppressed due to the high triplet energy of 2.90 eV. The triplet energy of the FPCA was high enough for exciton blocking, although it was slightly lower than that of the FPCC. The FPCC was also effective for triplet exciton blocking, but rather poor hole injection properties degraded the efficiency of the deep-blue PHOLEDs.

Similarly, the FPCC and FPCA were also applied as the HTMs in green PHOLEDs. Device data are presented in Figure 8. The current density and luminance of the green PHOLEDs showed the same tendency as that of deep-blue PHOLEDs. The quantum efficiency was also high in the FPCA device. The maximum quantum efficiency was 24.5%, and the quantum efficiency at 1000 cd/m² was 24.2%. There was little efficiency rolloff in the green PHOLED with the FPCA hole-transport layer. The power efficiency was also high; the maximum power efficiency and power efficiency at 1000 cd/m² were 58.5 lm/W and 50.1 lm/W, respectively. The FPCA hole-transport layer was also very effective in green PHOLED, because of good hole injection and suppressed triplet exciton quenching. Detailed device data are summarized in Table 2.

CONCLUSIONS

In conclusion, thermally stable high-triplet-energy hole-transport materials (HTMs), based on an 8H-indolo[3,2,1-de]-acridine (FPC) core, were synthesized and they enhanced the quantum efficiency of the deep-blue and green phosphorescent organic light-emitting diodes (PHOLEDs) to over 20%. The FPC-based HTMs showed high glass-transition temperatures (over 140 °C). Therefore, stable HTMs for deep-blue PHOLED application could be successfully developed, and they may improve the device stability in practical applications.

AUTHOR INFORMATION

Corresponding Author

*Tel.: 82-31-8005-3585. Fax: 82-31-8005-3585. E-mail: leej17@dankook.ac.kr.

REFERENCES

- (1) Baldo, M. A.; O'Brien, D. F.; You, Y.; Shoustikov, A.; Sibley, S.; Thompson, M. E.; Forrest, S. R. *Nature* **1998**, *395*, 151.
- (2) Adachi, C.; Baldo, M. A.; Thompson, M. E.; Forrest, S. R. *J. Appl. Phys.* **2001**, *90*, 5048.
- (3) Su, S.-J.; Tanaka, D.; Li, Y.-J.; Sasabe, H.; Takeda, T.; Kido, J. *Org. Lett.* **2008**, *10*, 941.
- (4) Xiao, L.; Su, S.-J.; Agata, Y.; Lan, H.; Kido, J. *Adv. Mater.* **2009**, *21*, 1271.
- (5) Chopra, N.; Lee, J.; Zheng, Y.; Eom, S.-H.; Xue, J.; So, F. *Appl. Phys. Lett.* **2008**, *93*, 143307.
- (6) Su, S. -J.; Chiba, T.; Takeda, T.; Kido, J. *Adv. Mater.* **2008**, *20*, 2125.
- (7) Sasabe, H.; Gonmori, E.; Chiba, T.; Li, Y.-J.; Tanaka, D.; Su, S.-J.; Takeda, T.; Pu, Y.-J.; Nakayama, K.; Kido, J. *Chem. Mater.* **2008**, *20*, 5951.
- (8) Holmes, R. J.; Forrest, S. R.; Sajoto, T.; Tamayo, A.; Djurovich, P. I.; Thompson, M. E.; Brooks, J.; Tung, Y.-J.; D'Andrade, B. W.; Weaver, M. S.; Kwong, R. C.; Brown, J. J. *Appl. Phys. Lett.* **2005**, *87*, 243507.
- (9) Kim, S. H.; Jang, J.; Lee, J. Y. *Appl. Phys. Lett.* **2007**, *90*, 223505.
- (10) Baldo, M. A.; Thompson, M. E.; Forrest, S. R. *Pure Appl. Chem.* **1999**, *71*, 2095.
- (11) Ikai, M.; Tokito, S.; Sakamoto, Y.; Suzuki, T.; Taga, Y. *Appl. Phys. Lett.* **2001**, *79*, 156.
- (12) Adamovich, V.; Cordero, S. R.; Djurovich, P. I.; Tamayo, A.; Thompson, M. E.; Andrade, B.; Forrest, S. R. *Org. Electron.* **2003**, *4*, 77.
- (13) Lee, J.; Chopra, N.; Eom, S.-H.; Zheng, Y.; Xue, J.; So, F.; Shi, J. *Appl. Phys. Lett.* **2008**, *93*, 123306.
- (14) Jeon, S. O.; Yook, K. S.; Joo, C. W.; Lee, J. Y. *Adv. Mater.* **2010**, *22*, 1872.

- (15) Jeon, S. O.; Yook, K. S.; Joo, C. W.; Lee, J. Y. *Adv. Funct. Mater.* **2009**, *19*, 3644.
- (16) Agata, Y.; Shimizu, H.; Kido, J. *Chem. Lett.* **2007**, *36*, 316.
- (17) Tanaka, D.; Agata, Y.; Takeda, T.; Watanabe, S.; Kido, J. *Jpn. J. Appl. Phys.* **2007**, *46*, L117.
- (18) Jeon, S. O.; Lee, J. Y. *Tetrahedron* **2010**, *66*, 7295.